Effect of geometrical rotation on conductance fluctuations in graphene quantum dots

2013 J. Phys.: Condens. Matter 25 105802

(http://iopscience.iop.org/0953-8984/25/10/105802)

IOP PUBLISHING JOURNAL OF PHYSICS: CONDENSED MATTER
J. Phys.: Condens. Matter **25** (2013) 105802 (7pp) doi:10.1088/0953-8984/25/10/105802

Effect of geometrical rotation on conductance fluctuations in graphene quantum dots

Lei Ying[1], Liang Huang[1,2], Ying-Cheng Lai[1,3] and Yan Zhang[4]

[1] School of Electrical, Computer, and Energy Engineering, Arizona State University, Tempe, AZ 85287, USA
[2] Institute of Computational Physics and Complex Systems, and Key Laboratory for Magnetism and Magnetic Materials of MOE, Lanzhou University, Lanzhou, Gansu 730000, People's Republic of China
[3] Department of Physics, Arizona State University, Tempe, AZ 85287, USA
[4] Institute of Theoretical Physics, Lanzhou University, Lanzhou, Gansu 730000, People's Republic of China

E-mail: lying5@asu.edu

Received 28 September 2012, in final form 7 January 2013
Published 8 February 2013
Online at stacks.iop.org/JPhysCM/25/105802

Abstract
Conductance fluctuations are ubiquitous in quantum transport through nanoscale devices, and how to modulate or control the fluctuation patterns is of considerable interest. We use two-terminal graphene devices as a prototypical system and articulate a scheme based on geometrical rotation of the device to effectively modulate the conductance fluctuations. To facilitate a systematic calculation of the conductance as a function of the Fermi energy and the rotation angle, we use a layer-by-layer based, recursive non-equilibrium Green's function approach, which is demonstrated to be computationally extremely efficient. Our study indicates that relative rotation of the device, which is experimentally feasible, can markedly affect the degree of conductance fluctuations, and we provide physical explanations of this behavior based on the emergence of edge states.

(Some figures may appear in colour only in the online journal)

1. Introduction

Quantum transport is fundamental to the development of nanoscale devices. Given a nanostructure, a large number of factors can affect the quantum-transport dynamics, such as the Fermi energy, the geometrical shape of the dot, external electrical and/or magnetic field, etc [1, 2]. Devising effective, experimentally feasible methods to modulate or control quantum transport is a problem of great interest at the present.

Key quantities underlying many quantum-transport processes are the conductances. Consider a two-dimensional nanoscale device such as a graphene [3–5] quantum dot or a more traditional semiconductor 2DEG (two-dimensional electron gas) structure [1]. When the device is connected through electron waveguides (or leads) to electron reservoirs (i.e., contacts) to form a circuit, various conductances can be defined with respect to voltage biases among the contacts together with the corresponding currents. Hall conductance in the presence of a perpendicular magnetic field is one such example. At low temperatures the conductances can be related to the corresponding quantum transmission [6], which depends on the electronic and device parameters. As a result, the conductances will also depend on these parameters. In the common situation in nanoscience, where the size of the device is less than the phase-relaxation length, quantum interference is important, which can lead to significant fluctuations in the conductances with respect to the parameter variations [7]. A critical issue is how the conductance-fluctuation pattern may be modulated or controlled. In this regard, a recent work has suggested the idea of exploiting classical transient chaos for quantum conductance modulation [8][5].

[5] The basic idea can be explained by using a quantum-dot structure. It has been generally known that quantum pointer states, resonant states of long lifetime inside the dot [21], can cause sharp conductance fluctuations. When the corresponding classical dynamics is integrable, there are stable periodic orbits in the phase space, about which highly localized quantum resonant states, or quantum pointer states, can form. When the classical dynamics becomes fully chaotic, no stable periodic orbits can exist, reducing significantly the probability for pointer states to exist. As a result, conductance fluctuations become smooth. If the degree of chaos can be experimentally adjusted, the quantum conductance-fluctuation patterns can then be modulated in a desirable manner.

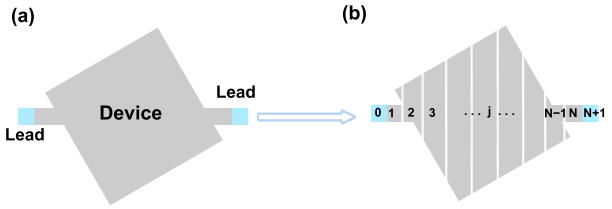

Figure 1. (a) Schematic illustration of a graphene quantum dot. (b) For a square quantum dot tilted with respect to the orientation of the left and right semi-infinite leads, construction of layer-based tight-binding Hamiltonians for recursive Green's function calculation. The device consists of layer 1 to layer N, while the left lead is from $-\infty$ to layer 0 and the right lead is from layer $N+1$ to ∞.

In this paper, we propose and computationally test a practical scheme to modulate quantum conductance fluctuations in nanoscale transport devices. We focus on graphene quantum dots. A dot structure typically consists of a device area of certain geometrical shape, such as a rectangle, and a number of leads connected to the device. Consider the common setup where a pair of semi-infinite, co-linear leads are connected to the device on the left- and right-hand side, respectively, as shown schematically in figure 1. Our basic idea is to exploit the relative orientation between the device and the leads to modulate conductance fluctuations. For example, figure 2(a) shows a situation where the device has been rotated with respect to the leads by an angle θ. For different angles, the conductance-fluctuation patterns can be quite different. In particular, when a physical parameter such as the Fermi energy E is varied, conductance G changes accordingly. For different values of θ, the fluctuation patterns of G with E will in general be different. It is convenient to write $G(E;\theta)$. For a fixed value of θ, the degree of the fluctuating behavior of the conductance with E can be characterized by the standard autocorrelation function

$$C(\Delta E,\theta)=\frac{\langle(G(E;\theta)-\bar{G})(G(E+\Delta E;\theta)-\bar{G})\rangle}{\langle[G(E;\theta)-\bar{G}]^2\rangle}, \quad (1)$$

where ΔE is a small energy interval, $\bar{G}$ is the mean of conductance, and the average $\langle\cdot\rangle$ is taken over a large energy interval. The half-width of $C(\Delta E,\theta)=0.5$, denoted by ε, will depend on the device angle θ, so we write $\varepsilon(\theta)$. Our hypothesis is that ε will depend markedly on θ, meaning that the degree of the conductance fluctuations can be effectively modulated by varying θ.

In order to test the hypothesis, we study a rectangular graphene quantum dot as a prototypical system, and use the standard tight-binding Hamiltonian and non-equilibrium Green's function approach [6] to calculate the conductance. To facilitate computations to gain high efficiency, especially for dots of relatively large sizes under systematically varying orientations, we develop a layer-based non-equilibrium Green's function approach, which decomposes the whole dot region into successive layers perpendicular to the direction of the semi-infinite leads and then calculates the Green's function of individual layers, one after another. This allows the conductance of arbitrarily large dots to be computed in an extremely efficient manner, insofar as the number of atoms in each layer is not prohibitively large, which is usually the case for typical graphene quantum dots of experimental interest. Our systematic computations reveal that the degree of conductance fluctuations can be modulated by geometrical rotations.

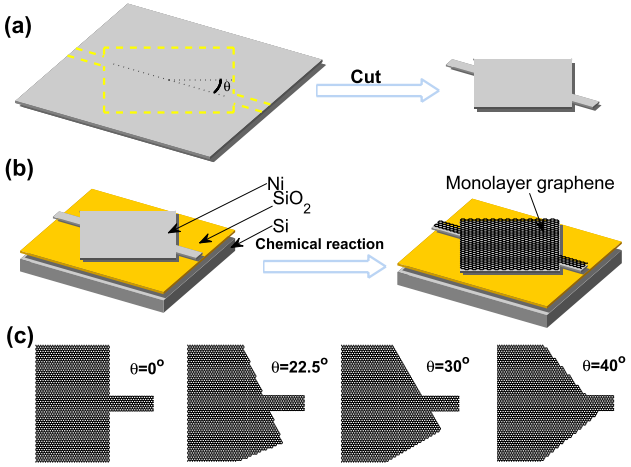

Figure 2. (a) Schematic diagram: a square graphene device with two leads is generated by cutting into a large graphene sheet. The angle θ is adjustable. (b) Typical process of experimental graphene growth. Left are three nano-layers made of Si, SiO_2, Ni, respectively. The nickel layer is shaped as device and lead geometry. The layers are heated to 1000 °C with flowing reaction gas (CH_4/H_2/Ar) mixtures. After cooling down to room temperature, a mono-layer graphene is pasted on upper layer. Etching the Ni and SiO_2 layers makes the graphene device fall down on the Si layer. (c) Local atomic configurations near a device-lead interface for $\theta = 0°$, 22.5°, 30° and 40°.

In section 2, we describe our layer-based recursive Green's function method for efficient computation of conductance fluctuations at arbitrary rotation angles. In section 3, we demonstrate that device rotation can be used to modulate the conductance-fluctuation pattern. Conclusions are presented in section 4.

2. Experimental scheme and layer-based recursive Green's function approach to conductance computation

A graphene device can be formed by cutting into a large graphene sheet, as shown in figure 2. While graphene sheet can be obtained by repeatedly peeling from multi-layer graphite [3], the chemical vapor-deposition (CVD) method [4, 9] can be used to grow a graphene device into any desirable shape, greatly facilitating the interaction between theoretical and experimental research. A possible scheme of experimentally realizing our system is as follows. A number of Ni layers are first cut into the desired geometries with rotation angles θ systematically varying from $-\pi/4$ to $\pi/4$, as shown in figure 2(a). Next, the Ni layers are placed on SiO_2/Si layers and processed chemically, as shown in figure 2(b). Graphene devices with pre-determined rotational angles are then synthesized, which are ready for conductance measurement.

At low temperatures, the conductance G of a quantum dot is proportional to the quantum transmission T, as given by the Landauer formula [6, 10]:

$$G(E) = (2e^2/h)T(E). \tag{2}$$

Transmission is usually calculated by the non-equilibrium Green's function (NEGF) method [11]. For a graphene quantum-dot system consisting of a device region and two semi-infinite leads (left lead and right lead) as shown in figure 1(a), the transmission can be conveniently calculated through the self-energies [6]. In particular, let H_{D} be the finite Hamiltonian matrix describing the device in the tight-binding framework. The Green's function of the device is given by

$$G_{\mathrm{D}} = (EI - H_{\mathrm{D}} - \Sigma_{\mathrm{L}} - \Sigma_{\mathrm{R}})^{-1}, \tag{3}$$

where Σ_{L} and Σ_{R} are the self-energies associated with the left and right leads, respectively. Let $V_{\mathrm{L,R}}$ be the coupling matrix between the left (right) lead with the device, the self-energies can be calculated by the following equations [13]:

$$\Sigma_{\mathrm{L,R}} = V_{\mathrm{L,R}}^{\dagger} G_{\mathrm{L,R}} V_{\mathrm{L,R}}, \tag{4}$$

where $G_{\mathrm{L,R}}$ are Green's functions for the left and right leads. The transmission is then given by

$$T(E) = \mathrm{Tr}(\Gamma_{\mathrm{L}} G_{\mathrm{D}} \Gamma_{\mathrm{R}} G_{\mathrm{D}}^{\dagger}), \tag{5}$$

where $\Gamma_{\mathrm{L,R}} \equiv \mathrm{i}(\Sigma_{\mathrm{L,R}} - \Sigma_{\mathrm{L,R}}^{\dagger})$. The local density of states (LDS) for the device is

$$\rho_{\mathrm{D}} = -\frac{1}{\pi}\mathrm{Im}[\mathrm{diag}(G_{\mathrm{D}})]. \tag{6}$$

Although the above procedure is standard, for large graphene quantum dots (e.g., length scale of 100 nm), the size of the Hamiltonian matrix H_{D} will be large, making the computation extremely demanding, especially in terms of the memory requirement. We are thus led to develop a layer-by-layer type of recursive Green's function (RGF) method to calculate the transmission and the local density of states. The basic idea is to divide a given (large) device into smaller units or layers. The specific way to choose the division can be highly flexible, depending on the geometrical shape of the device region. A well-designed, physically meaningful division scheme can help accelerate the computation tremendously. An example is shown in figure 1(b), where a square device tilted with respect to the orientation of the left and right leads (horizontal direction) is divided into N layers. The left and right leads can be conveniently labeled as layer 0 and layer $N+1$, respectively. In this RGF method, each layer j ($j = 1, \ldots, N$) is considered as a separated device and its nearest neighboring layers $j-1$ and $j+1$ are regarded as the local left and right 'leads' connecting to the device, respectively. The Green's function G_j for layer j is determined by the Fermi energy and the self-energies from its 'leads'. Carrying out the calculation of the Green's function layer-by-layer, we can assemble the Green's function for the original (large) device.

A detailed formulation of RGF method is the following. Starting from the left side of the device, the self-consistent Dyson equation $\Sigma_{\mathrm{l}} = V_0^{\dagger}(E - H_0 - \Sigma_{\mathrm{l}})^{-1}V_0$ solves the self-energy of layer 1, denoted by $\Sigma_{\mathrm{l},1}$, due to the left lead, where V_0 is the coupling matrix between the first layer of the device and the left lead. The Green's function of layer 1, taking into account the self-energy $\Sigma_{\mathrm{l},1}$, is then given by

$$G_{\mathrm{l},1}(E) = (EI - H_{11} - \Sigma_{\mathrm{l},1})^{-1}, \tag{7}$$

where H_{11} is the Hamiltonian of layer 1. Similarly, the self-energy of layer 2 due to its local left lead, which is in fact layer 1, is given by

$$\Sigma_{\mathrm{l},2} = H_{21}G_{\mathrm{l},1}(E)H_{12} = H_{12}^{\dagger}G_{\mathrm{l},1}(E)H_{12}, \tag{8}$$

where H_{12} is the coupling matrix from layer 2 to layer 1. We can thus obtain the Green's function of layer 2 taking into account the self-energy from the 'new' left lead, which now includes layer 1 (non-uniform leads). Repeating this recursive procedure, we can obtain the self-energies of layers 3, 4, and so on. In general, for layer $j = 1, \ldots, N-1$, we can use the following equation repeatedly:

$$G_{\mathrm{l},j}(E) = (EI - H_{jj} - \Sigma_{\mathrm{l},j})^{-1}, \tag{9}$$

$$\Sigma_{\mathrm{l},j+1} = H_{j+1,j}G_{\mathrm{l},j}(E)H_{j,j+1}, \tag{10}$$

to get the self-energy $\Sigma_{\mathrm{l},N}$ for the left lead of layer N. Similar to the case of the left lead, a Dyson equation for the right lead also exists (for the first layer of the device in contact with the right lead), from which we can obtain the self-energy of layer N due to the right lead, $\Sigma_{\mathrm{r},N}$. Regarding the layer N itself as a device, we can calculate its Green's function

$$G_N(E) = (EI - H_{NN} - \Sigma_{\mathrm{l},N} - \Sigma_{\mathrm{r},N})^{-1}, \tag{11}$$

and its coupling matrices $\Gamma_{\mathrm{l}} = \mathrm{i}(\Sigma_{\mathrm{l},N} - \Sigma_{\mathrm{l},N}^{\dagger})$ and $\Gamma_{\mathrm{r}} = \mathrm{i}(\Sigma_{\mathrm{r},N} - \Sigma_{\mathrm{r},N}^{\dagger})$. The transmission T of this layer, which is the same as the transmission for the original whole device, is given by

$$T(E) = \mathrm{Tr}(\Gamma_{\mathrm{l}}G_N\Gamma_{\mathrm{r}}G_N^{\dagger}). \tag{12}$$

The local density of states (LDS) can also be calculated using the RGF method in a layer-by-layer formulation. In particular, for layer j, one can compute the self-energy $\Sigma_{\mathrm{l},j}$ by using equations (9) and (10) recursively. Similarly, starting from the right-hand side, by repeatedly applying

$$G_{\mathrm{r},j}(E) = (EI - H_{jj} - \Sigma_{\mathrm{r},j})^{-1}, \tag{13}$$

$$\Sigma_{\mathrm{r},j-1} = H_{j-1,j}G_{\mathrm{r},j}(E)H_{j,j-1}, \tag{14}$$

we get the self-energies $\Sigma_{\mathrm{r},j}$ from the right lead for layer j. The Green's function $G_j(E)$ for this layer taking into account both left and right leads is $G_j(E) = (EI - H_{jj} - \Sigma_{\mathrm{l},j} - \Sigma_{\mathrm{r},j})^{-1}$. The LDS for this layer is then

$$\rho_j = -\frac{1}{\pi}\mathrm{Im}[\mathrm{diag}(G_j)], \tag{15}$$

and the LDS for the whole device is given by

$$\rho = [\rho_1, \rho_2, \ldots, \rho_N]. \tag{16}$$

Note that the Green's functions obtained in equations (9) and (13) are incomplete in a sense that they incorporate the

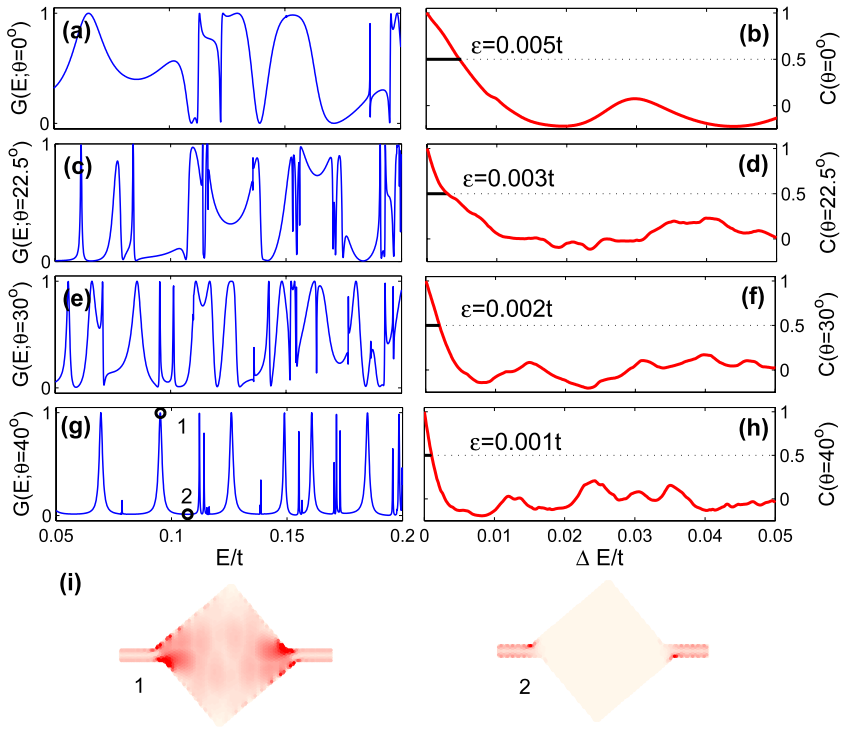

Figure 3. For a square device of side length $L = 60.5a_0$, where a_0 is the lattice constant of graphene, dimensionless conductance $G(E)$ as a function of the Fermi energy, where the conductance is normalized by $G_0 = 2e^2/h$, and the corresponding autocorrelation curves: ((a), (b)) $\theta = 0$, ((c), (d)) $\theta = 22.5°$, ((e), (f)) $\theta = 30°$ and ((g), (h)) $\theta = 45°$. (i) LDS patterns corresponding to the black circles in (g).

self-energies from either the left or the right lead and thus cannot be used to derive the LDS.

The merits of this layer-based recursive RGF method lie in its time and memory efficiency for large device simulations, its high accuracy, and the flexibility to treat devices of arbitrarily geometrical shape. The method is not limited to the calculation of transport properties for open systems. In fact, by imposing the zero-contact condition at the boundaries of the leads, this RGF method can be adopted to closed system calculations of eigenvalues and eigenstates. Extensive tests indicate that the recursive NEGF method outperforms the conventional NEGF method in the computational efficiency by up to three orders of magnitude. For example, the ratio of the CPU times required for calculating the LDS patterns in figure 5 by using the conventional method and the recursive method is about 800, which is typical for conductance and LDS calculations reported in this paper.

3. Results

To be concrete, we consider a square-shaped graphene device of side length $L = 60.5a_0$, where $a_0 = \sqrt{3}a \approx 0.246$ nm is the lattice constant and a denotes the C–C bond length in graphene. Two leads of width $W = 11a$ are connected to the central regions of the left and right sides of the device, where the angle θ is a control parameter that can be varied in the range $[-\pi/4, \pi/4]$. The leads are graphene nano-ribbons that can have either zigzag or armchair boundaries. For a fixed value of θ, we calculate the conductance $G(E)$, normalized by $G_0 = 2e^2/h$, as a function of the Fermi energy E. Figure 3 shows the conductance-fluctuation patterns and the corresponding autocorrelation functions for $\theta = 0°, 22.5°, 30°$ and $40°$. We observe that rotation can affect the fluctuation pattern markedly. For example, for $\theta = 0°$, the conductance curve appears more smooth. For $\theta = 40°$, the fluctuations are sharper. The fluctuation patterns can be characterized by the autocorrelation functions in terms of the half-width ε. We have $\varepsilon = 0.005t$ for $\theta = 0°$, but it reduces to $\varepsilon = 0.001t$ for $\theta = 40°$, where t is the nearest-neighbor hopping energy of the graphene lattice.

We note that the conductance fluctuations in figure 3(g) are unusually strong as compared with other cases, in the sense that the conductance is nearly zero for most energy values and reaches maximum values for relatively fewer energy values, and the transitions between near-zero and maximum values appear quite abrupt with respect to change in the energy. The main reason is that, for relatively large rotational angles (e.g., $\theta = 40°$), the boundary mismatch between the graphene leads and device induces strong backscattering except for those energy values where edge states can form. The LDS pattern of an edge state is shown in figure 3(i) on the left-hand side, while a strong backscattering state is shown on the right-hand side where we observe essentially zero electron density in the device region.

To obtain a comprehensive picture, we show in figure 4(a) a contour plot of the conductance in the two-dimensional parameter space (θ, E), where the leads of the rotated device have zigzag boundaries. We observe that, for θ in different regions, the conductance-fluctuation patterns with the Fermi energy can be characteristically different, indicating the role of device rotation in modulating the conductance fluctuations. From a different standpoint, for a fixed Fermi energy, the

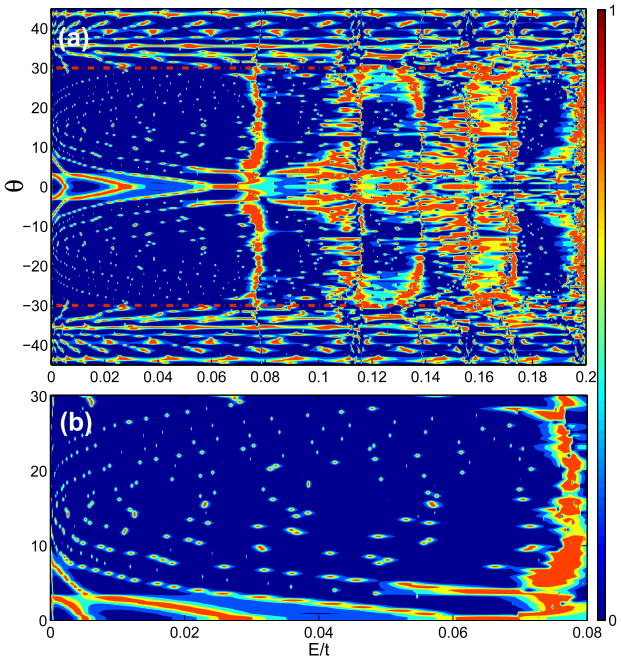

Figure 4. For zigzag leads and a device with zigzag boundary at $\theta = 0$, contour plot of the normalized conductance in the two-dimensional parameter plane (θ, E): (a) full-range plot where the color represents the conductance value. The red dashed lines divide the conductance-fluctuation pattern into three regions, (b) magnification of part of (a).

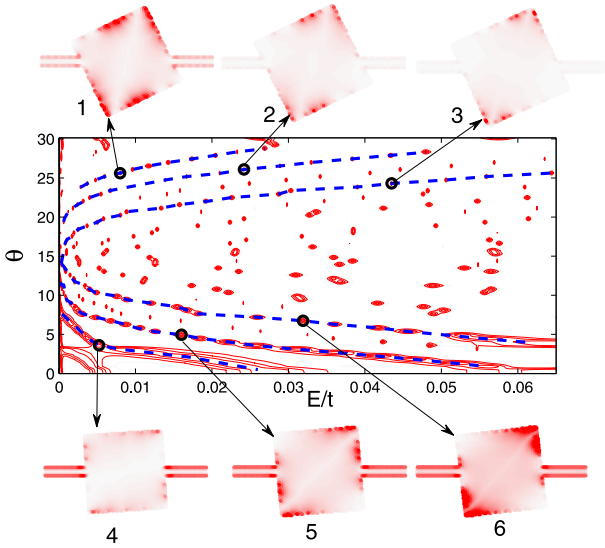

Figure 5. Transmission contours about angle θ and energy E. The blue dashed lines link the transmission peaks. The black circles represent the LDS patterns of the entire parabolic blue lines. The energies for the LDS patterns 1, 2, 3, 4, 5, and 6 are $E_1 = 0.008t$, $E_2 = 0.0242t$, $E_3 = 0.0435t$, $E_4 = 0.052t$, $E_5 = 0.016t$ and $E_6 = 0.0319t$, respectively, and the corresponding angles are $\theta_1 = 25.65°$, $\theta_2 = 26.10°$, $\theta_3 = 24.30°$, $\theta_4 = 3.60°$, $\theta_5 = 4.95°$ and $\theta_6 = 6.75°$.

conductance can be viewed to fluctuate with θ. In particular, in the low-energy regime, the conductance varies relatively slowly with θ, but significant fluctuations of the conductance with θ occur in the large energy regime. Approximately, we can divide the contour plot in figure 4(a) into three distinct regions: $\theta < -\pi/6$, $-\pi/6 \leq \theta \leq \pi/6$, and $\theta > \pi/6$, which are marked by the red dashed lines. The critical angles $\pm\pi/6$ arise because of the hexagonal lattice structure of the leads (graphene ribbons) with zigzag boundaries. In the range $-\pi/6 \leq \theta \leq \pi/6$, there are two symmetrical regions in the contour plot with nearly uniformly low-conductance values and only a few small regular islands of high conductance values in the low Fermi-energy region ($E \leq 0.08t$).

In the two mostly low-conductance areas, the rare points of high conductance values form approximately parabolic curves, as can be seen from the contour plot in figure 4(b). As the square device is rotated, its boundary changes from totally zigzag or totally armchair type at $\theta = 0$ to a mixture of both. For a given value of θ, only for a few energy values are the conductance values appreciable. The pattern of relatively high values of the conductance is also symmetric with respect to $\theta = \pi/12$. The reason is that, when the rotation angle reaches $\theta = \pi/6$, the orientation of the leads coincides with the armchair boundary of the device, and the angle $\pi/12$ corresponds to the 'most' mixed boundaries. In fact, the parabolic curves in figure 4(b) are a consequence of the formation of the edge states in the graphene device, as shown in figure 5. Along each parabolic curve, although the connecting angle between the device and the leads is systematically changed, the LDS patterns indicate localization of electronic states about the corners of devices, which are similar to each other. For example, in figure 5, patterns 1 and 4, patterns 2 and 5, and patterns 3 and 6 exhibit similar edge states. In the black area in figure 4, there are no edge states.

When the ribbons have armchair boundaries and the device's boundaries are also armchair initially (at $\theta = 0$), we observe qualitatively similar patterns to those in figure 4(a), but the trend of conductance changes is opposite, as shown in figure 6. The reason can be attributed to the distinct electronic behaviors for different types of boundaries. In particular, at low energy, electrons are localized near the zigzag edges [12], so a change from zigzag to armchair boundary can reduce the conductance gradually, as can be seen from the three LDS patterns in figure 7. Conceptually, the zigzag boundaries act as channels, while the armchair boundaries behave as barriers to these channels. For $\theta = 30°$ and the initial zigzag device connected to zigzag leads, the electrons travel through the channel smoothly to pass the device, giving rise to large conductances, as the middle LDS pattern in figure 7(b) indicates, where the light blue dash lines mark the potential channels. Hence, as shown in figure 4(a), the average conductance at $\theta = 30°$ is larger than those at other angles. In a graphene system, the Fermi energy follows $E \sim k \sim 1/\lambda$, where λ is the electron wavelength. When the device is rotated away from the initial setting, say to $\theta = 22.5°$, a large number of barriers (armchair boundaries) arise, as indicated in figure 2(b), which the electrons cannot cross. Indication of this behavior can also be seen from the left LDS pattern in figure 7, where few electrons extend into the device due to the barriers. When the angle is changed, cases such as that illustrated by the third LDS pattern in figure 7 can arise.

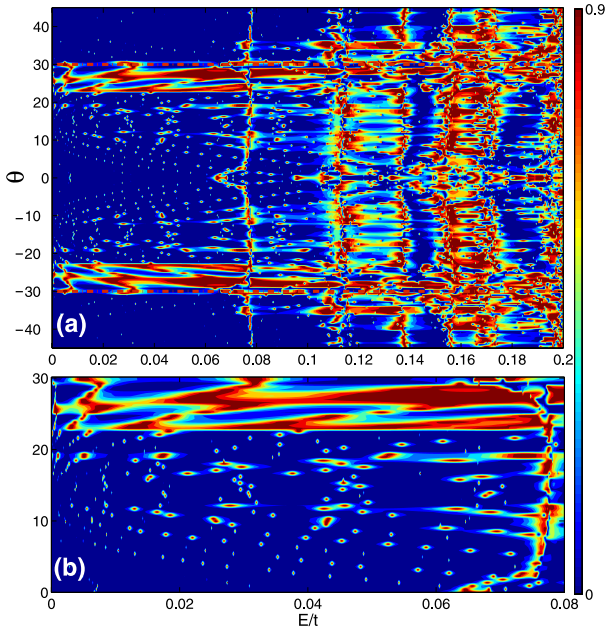

Figure 6. For armchair leads and a device with armchair boundary at $\theta = 0$, contour plot of the normalized conductance in the two-dimensional parameter plane (θ, E): (a) full-range plot where the color represents the conductance value. The red dashed lines divide the conductance-fluctuation pattern into three regions, (b) magnification of part of (a).

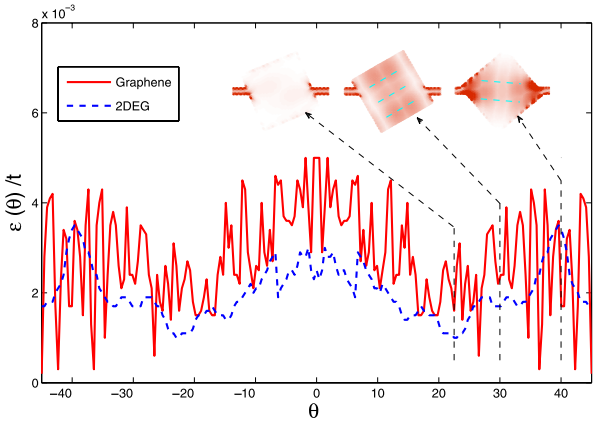

Figure 7. For a system with zigzag boundaries, half-width of the energy autocorrelation function versus the angle of rotation θ. Result from a conventional semiconductor 2DEG system of the same geometry and size is included for comparison (dashed curve). Three representative LDS patterns for Fermi energy $E = 0.07t$ and $\theta = 0°$, 22.5° and 40° are shown to illustrate the conducting channels.

To quantify the effect of rotation on the conductance-fluctuation pattern, we calculate the energy autocorrelation function $C(\Delta E, \theta)$ for each fixed value of rotation angle θ and plot the half-width ε as a function of θ. The energy range for performing the average in equation (1) is chosen to be $[0.05t, 0.1t]$. The result is shown in figure 7, For comparison, the result from a 2DEG system of the same geometry and size (corresponding effectively to a square-lattice system in the tight-binding framework) is also included. We see that, for the graphene system, the half-width depends sensitively on the rotation angle, especially for large angles, although the dependence is relatively weak in the angle range $\theta \in [-\pi/6, \pi/6]$. The sensitivity originates from the fact that, in graphene, electron mobility is extremely direction-dependent. As a result, a slight change in the graphene lattice orientation will result in a drastic change in the conductance. In fact, it is a general property of graphene that small structural perturbations at the atomic level, such as adding or removing one atom, affect the conductance significantly [13, 14]. In contrast, for the corresponding 2DEG system, the dependence of the half-width on the rotation angle is much more smooth, due to the isotropic nature of the electrons' traveling direction.

An issue is the effect of impurity or disorder [15, 16]. When a small amount of impurity is present, conductance may be enhanced on average because the random scattering induced by the impurity can break the localized, resonance-type of LDS patterns [16] that typically lead to extremely sharp conductance fluctuations. However, for large amounts of impurity, strong localization can set in, reducing the conductance significantly. Thus an optimal amount of impurity can maximize the conductance [16]. For a fixed amount of impurity in the device, the average value of the conductance may change but the variations of the conductance with respect to device rotation are expected to remain qualitatively the same.

Another interesting issue concerns the interplay between the conductance-fluctuation pattern and the size of the quantum dot. This is especially relevant when a perpendicular magnetic field is present. In particular, for a quantum dot of given geometrical shape, the conductance can vary periodically with the strength of the magnetic field, the frequency of which, the so-called magnetic frequency, depends on the dot size [17], and in fact follows a linear scaling relation [18, 19]. The origin of the scaling can be attributed to the interplay between the Landau levels and some pronounced quantum pointer states [20]. In our case, rotation of the quantum-dot device can lead to the emergence of different groups of quantum pointer states. Thus, in the presence of a magnetic field, the magnetic frequency is expected to depend on the dot size linearly but the associated slope will depend on the angle of rotation.

Varying the device aspect ratio W/L, insofar it is small, does not affect the effect of device rotation on conductance-fluctuation patterns. When the shape of the device is changed, the fluctuation pattern may change characteristically. For example, if the shape is such that the corresponding classical dynamics is chaotic, the conductance fluctuations will be more smooth as compared with the case where the classical dynamics is regular ([8], see footnote 5). However, rotation can still have a significant effect on the conductance-fluctuation pattern, regardless of the geometric shape of the quantum dot.

4. Conclusion

The conductance of a nanoscale quantum dot depends on many parameters, such as the Fermi energy, the strength of

external magnetic field (if there is one), and the details of the geometry of the structure, etc. Conductance fluctuations are thus an issue of both fundamental interest [7] and practical significance. Especially, in the development of nanoscale quantum-transport device for circuit and sensor implementations, it is desirable to be able to modulate the conductance-fluctuation patterns depending on the specific application requirements. Recently it has been suggested that classical chaos can be exploited to control the statistical characteristics of conductance fluctuations in both semiconductor 2DEG and graphene quantum dots ([8], see footnote 5).

We have suggested an experimentally realizable scheme to modulate conductance fluctuations in quantum-dot devices. Our idea is to exploit geometrical rotation of the device relative to the leads, which is tested computationally using two-terminal graphene and conventional semiconductor 2DEG systems. To overcome the challenge of computing systematically the conductance in multiple parameter space (e.g., the Fermi energy and the device rotation angle) for relatively large devices, we use a layer-based recursive Green's function method. Our study indicates that geometrical rotation can have a drastic effect on the autocorrelation width of the conductance-fluctuation pattern, and the dependence is more sensitive for the graphene device. Qualitatively, the mechanism of modulation can be understood by the emergence of the edge states in graphene systems. Control of quantum-transport dynamics, especially in graphene systems, is a problem of great importance in the development of all sorts of nanoscale devices, and our geometry-based method represents a simple but effective scheme in this pursuit.

Acknowledgments

This work was supported by AFOSR under Grant No. FA9550-12-1-0095 and by ONR under Grant No. N00014-08-1-0627. LH was also supported by NSFC under Grant No. 11005053 and by the Fundamental Research Funds for the Central University under Grant No. lzujbky-201022-19.

References

[1] Ferry D K and Goodnick S M 2000 *Transport in Nanostructures* (Cambridge: Cambridge University Press)
[2] Di Ventra M 2008 *Electrical Transport in Nanoscale Systems* (Cambridge: Cambridge University Press)
[3] Novoselov K S, Geim A K, Morozov S V, Jiang D, Zhang Y, Dubonos S V, Grigorieva I V and Firsov A A 2004 *Science* **306** 666
[4] Berger C, Song Z, Li T, Li X, Ogbazghi A Y, Feng R, Dai Z, Marchenkov A N, Conrad E H, First P N and de Heer W A 2004 *J. Phys. Chem.* B **108** 19912
[5] Novoselov K S, Geim A K, Morozov S V, Jiang D, Katsnelson M I, Grigorieva I V, Dubonos S V and Firsov A A 2005 *Nature* **438** 197
Zhang Y, Tan Y-W, Stormer H L and Kim P 2005 *Nature* **438** 201
Castro Neto A H, Guinea F, Peres N M R, Novoselov K S and Geim A K 2009 *Rev. Mod. Phys.* **81** 109
Peres N M R 2010 *Rev. Mod. Phys.* **82** 2673
Das Sarma S, Adam S, Hwang E H and Rossi E 2011 *Rev. Mod. Phys.* **83** 407
[6] Datta S 1995 *Electronic Transport in Mesoscopic Systems* (Cambridge: Cambridge University Press)
[7] Jalabert R A, Baranger H U and Stone A D 1990 *Phys. Rev. Lett.* **65** 2442
Ketzmerick R 1996 *Phys. Rev.* B **54** 10841
Taylor R P *et al* 1997 *Phys. Rev. Lett.* **78** 1952
Sachrajda A S, Ketzmerick R, Gould C, Feng Y, Kelly P J, Delage A and Wasilewski Z 1998 *Phys. Rev. Lett.* **80** 1948
Huckestein B, Ketzmerick R and Lewenkopf C H 2000 *Phys. Rev. Lett.* **84** 5504
Casati G, Guarneri I and Maspero G 2000 *Phys. Rev. Lett.* **84** 63
Crook R, Smith C G, Graham A C, Farrer I, Beere H E and Ritchie D A 2003 *Phys. Rev. Lett.* **91** 246803
[8] Yang R, Huang L, Lai Y-C and Grebogi C 2011 *Europhys. Lett.* **94** 40004
Yang R, Huang L, Lai Y-C and Pecora L M 2012 *Appl. Phys. Lett.* **100** 093105
[9] Berger C, Song Z and Li T 2004 *J. Phys. Chem.* B **108** 19912
Berger C, Song Z, Li X and First P N 2006 *Science* **312** 1191
Coraux J, N'Diaye A T, Busse C and Michely T 2008 *Nano Lett.* **8** 565
Pan Y, Zhang H, Shi D, Sun J, Du S, Liu F and Gao H-J 2008 *Adv. Mater.* **20** 1
Li X, Cai W and An J 2009 *Science* **324** 1312
Kim K S, Zhao Y and Jang H 2009 *Nature* **457** 706
[10] Landauer R 1970 *Phil. Mag.* **21** 863
[11] Lee P A and Fisher D S 1981 *Phys. Rev. Lett.* **47** 882
Ando T 1991 *Phys. Rev.* B **44** 8017
[12] Muñoz-Rojas F, Jacob D, Fernández-Rossier J and Palacios J J 2006 *Phys. Rev.* B **74** 195417
[13] Li T C and Lu S 2008 *Phys. Rev.* B **77** 085408
Huang L, Lai Y-C, Ferry D K, Akis R and Goodnick S M 2009 *J. Phys.: Condens. Matter* **21** 344203
Xu H and Heinzel T 2008 *Phys. Rev.* B **77** 245401
[14] Yan J-Y, Zhang P and Sun B 2009 *Phys. Rev.* B **79** 115403
[15] Zhang Y-Y, Hu J, Bernevig B A, Wang X R, Xie X R and Liu W M 2010 *Phys. Status Solidi* a **207** 2726
[16] Jiang L-L, Huang L, Yang R and Lai Y-C 2010 *Appl. Phys. Lett.* **96** 262114
[17] Bird J P *et al* 1997 *Chaos Solitons Fractals* **8** 1299
Ferry D K, Bird J P, Akis R, Pivin D P Jr, Connolly K M, Ishibashi K, Aoyagi Y, Sugano T and Ochiai Y 1997 *Japan. J. Appl. Phys.* **36** 3944
Holmbert N, Akis R, Pivin D P Jr, Bird J P and Ferry D K 1999 *Semicond. Sci. Technol.* **13** A21
[18] Ujiie Y, Morimoto T, Aoki N, Ferry D K, Bird J P and Ochiai Y 2009 *J. Phys.: Condens. Matter* **21** 382202
[19] Ferry D K, Huang L, Yang R, Lai Y-C and Akis R 2010 *J. Phys.: Conf. Ser.* **220** 012015
[20] Ying L, Huang L, Lai Y-C and Grebogi C 2012 *Phys. Rev.* B **85** 245448
[21] Zurek W H 2003 *Rev. Mod. Phys.* **75** 715
Akis R, Bird J P and Ferry D K 2002 *Appl. Phys. Lett.* **81** 129
Ferry D K, Akis R and Bird J P 2004 *Phys. Rev. Lett.* **93** 026803